ACS APPLIED MATERIALS & INTERFACES

Research Article

www.acsami.org

# Nanostructured Hybrid Layered-Spinel Cathode Material Synthesized by Hydrothermal Method for Lithium-Ion Batteries

Cong Liu, Zhiyuan Wang, Chunsheng Shi,* Enzuo Liu, Chunnian He, and Naiqin Zhao

School of Materials Science and Engineering and Tianjin Key Laboratory of Composites and Functional Materials, Tianjin University, Tianjin 300072, China

Collaborative Innovation Center of Chemical Science and Engineering, Tianjin 300072, China

Supporting Information

**ABSTRACT:** Nanostructured spinel $LiMn_{1.5}Ni_{0.5}O_4$, layered $Li_{1.5}Mn_{0.75}Ni_{0.25}O_{2.5}$ and layered-spinel hybrid particles have been successfully synthesized by hydrothermal methods. It is found that the nanostructured hybrid cathode contains both spinel and layered components, which could be expressed as $Li_{1.13}Mn_{0.75}Ni_{0.25}O_{2.32}$. Diffraction-contrast bright-field (BF) and dark-field (DF) images illustrate that the hybrid cathode has well dispersed spinel component. Electrochemical measurements reveal that the first-cycle efficiency of the layered-spinel hybrid cathode is greatly improved (up to 90%) compared with that of the layered material (71%) by integrating spinel component. Our investigation demonstrates that the spinel containing hybrid material delivers a high capacity of 240 mAh $g^{-1}$ with good cycling stability between 2.0 and 4.8 V at a current rate of 0.1 C.

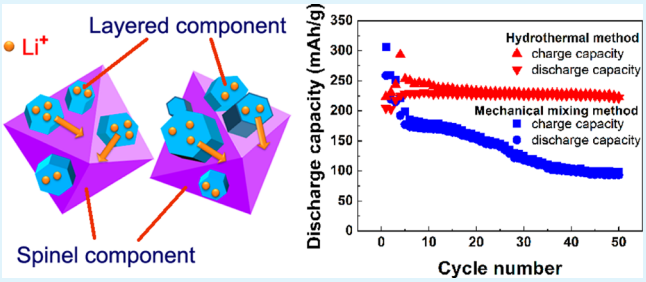


**KEYWORDS:** *layered-spinel hybrid cathode, lithium-ion battery, hydrothermal synthesis*

## 1. INTRODUCTION

In recent years, the lithium-ion batteries have been successfully used in the portable devices such as mobile phones, digital cameras, and laptop computers etc. However, the performance of lithium battery cannot entirely meet the requirements of electric vehicles (EV) and hybrid electric vehicles (HEV), which need high power and energy densities. The energy density of a lithium battery was determined by the cathode capacity and its operating voltage, so developing high energy, high voltage and low cost cathode materials has become the key factor for high-performance rechargeable lithium-ion batteries.[1−5]

Lithium-rich manganese-based material $Li_2MnO_3$−$LiMO_2$ (M = Mn, Ni, Co) with layered−layered structures has drawn a lot of attention recently since they were synthesized by Lu and Thackeray.[3,6] These materials seem to be among the most promising candidates for lithium-ion batteries and can provide very large specific capacity more than 250 mAh $g^{-1}$ when they are charged over 4.6 V or higher (>4.6 V vs. $Li^+$/Li).[7] Despite their ability to provide a significantly higher capacity, the layered cathode material has several limits, such as relatively poor rate capacities, low first cycle efficiency, and a significant voltage decay when continuously cycled to high potentials.[8] Spinel $LiNi_{0.5}Mn_{1.5}O_4$ is also a very promising material for its good cycling performance at room temperature and three-dimensional interstitial space permits fast diffusion of lithium ions. The main drawback of spinel $LiNi_{0.5}Mn_{1.5}O_4$ lies in a limited discharge capacity of ∼130 mAh $g^{-1}$.[9] So integrating a spinel component within $Li_2MnO_3$-based layered oxides to get new layered-spinel hybrid electrodes with obvious superiorities of the two components has been pursued by many research groups.[10] The spinel component here can offset the first-cycle coulombic inefficiency and offer the high rate capacity of the composite electrode. In addition, the nanostructure could improve the power density of Li-ion batteries by decreasing lithium ion transport path during delithiation and lithiation processes.[11−13] The methods for synthesizing layered-spinel composites mainly include co-precipitation method,[1,8−10,14,15] lithium ion-exchange method,[16,17] and spray pyrolysis method.[18,19] Hydrothermal process is a relatively low temperature process and has advantages of high crystallinity, high yield, homogeneous particle products, and narrow particle-size distributions, etc.[20] Hydrothermal synthesis has been used to prepare nanosized layered $LiMnO_2$−$Li_2MnO_3$ compounds and $Li[Ni_{0.2}Li_{0.2}Mn_{0.6}]O_2$ layered−layered nanowires.[11,20] To date, few investigations are concerned with hydrothermal synthesis of layered-spinel hybrids as cathode materials for lithium-ion batteries and the structure relationship between the two components.

In this paper, we developed one-step hydrothermal and calcination method to integrate a spinel component into $Li_2MnO_3$-based layered oxides. The structure, morphology and electrochemical properties of three structures: the spinel structure, layered-spinel hybrid and layered structure were

Received: March 3, 2014
Accepted: May 14, 2014
Published: May 14, 2014

   dx.doi.org/10.1021/am501280t | ACS Appl. Mater. Interfaces 2014, 6, 8363−8368

investigated thoroughly. Using spinel component to stabilize high capacity layered electrode, it is expected that the electrochemical performance of the layered-spinel hybrid cathode would be significantly improved.

## 2. EXPERIMENTAL SECTION

**2.1. Synthesis of Hybrid Layered-Spinel Cathode Material.** The three samples were synthesized from the same precursor ratio via hydrothermal method followed by calcinations. In a typical process 2.685 g of $LiOH{\cdot}H_2O$ (AR, Tianjin Weichen Chemical Reagent Company) was dissolved in 25 ml deionized water and then added slowly dropwise into an aqueous solution containing the required stoichiometric amounts of $MnSO_4{\cdot}H_2O$ (1.01 g), $NiSO_4{\cdot}6H_2O$ (0.525 g), $(NH_4)_2S_2O_8$ (1.36 g) (AR, Tianjin Kewei Chemical Reagent Company) under continuous stirring. Then, the layered-spinel hybrid sample was sealed in an autoclave and heated typically at 180 °C for 10 h, spinel $LiMn_{1.5}Ni_{0.5}O_4$ for 1 h and layered $Li_2MnO_3{-}LiMn_{0.5}Ni_{0.5}O_2$ for 24 h. Finally the precipitates of spinel sample and layered-spinel hybrid sample were filtered, washed, and then dried at 80 °C overnight. However, layered sample precipitate was stirred vigorously until dry. The obtained samples were ground by an agate mortar. Then the resulting powder were placed into an alumina crucible and calcined at 800 °C for 8 h in air to get the final products.

**2.2. Characterization.** A powder X-ray diffractometer (XRD, Bruker D8 ADVANCE) with a Cu-Ka radiation (1.5405 Å) in a range of 10°−90° was used to identify the crystal structure and phase composition. The morphological features and particle size of the powders were observed using a field emission scanning electron microscope (FE-SEM, HITACHI S4800) and a high-resolution transmission electron microscope (HRTEM, PHILIPS TECNAI G2F20). The Raman spectra were recorded via a Renishaw Raman spectroscopy system, using laser excitation at 512 nm from an argon ion laser source. Fourier transform infrared (FTIR, Tensor 27) spectra were recorded using a WQF-510 spectrometer. Nitrogen adsorption isotherms of the cathode materials were measured at 77 K using an autosorb iQ instrument (Quantachrome U.S.). The total surface area was calculated from the Brunauer−Emmett−Teller (BET) method and the pore size distribution data was calculated using the Barrett−Joyner−Halenda (BJH) method.

**2.3. Electrochemical Measurements.** Electrochemical properties were tested in CR2032 coin cells with lithium−metal anodes. The synthesized cathode materials were mixed with carbon black and poly(vinylidene fluoride) binder (PVDF) in *N*-methyl-2-pyrrolidinone solvent with a weight ratio of 80:10:10. After mixing thoroughly, the slurry was coated on an aluminum foil current collector, dried at 120 °C overnight in a vacuum oven and cut into a wafer with area of 1.13 $cm^2$. Coin cells were assembled in an argon-filled glove box with lithium metal as the counter electrode and reference electrode, Celgard 2300 polypropylene film as separator and 1 M $LiPF_6$ dissolving in ethylene carbonate (EC)/ethyl methyl carbonate (EMC)/dimethyl carbonate (DEC) (1:1:1 in volume) as electrolyte.

Galvanostatic charge/discharge tests were performed in a voltage range of 2.0-4.8 V with different current densities. The cyclic voltammetry (CV) tests were conducted using a CHI 660D electrochemical workstation between 2.0 and 4.8 V versus $Li^+/Li$ at a scan rate of 0.2 mV $s^{-1}$ at room temperature.

## 3. RESULTS AND DISCUSSION

**3.1. Morphology.** Figure 1 shows the particle morphologies of the spinel $LiMn_{1.5}Ni_{0.5}O_4$, layered $Li_{1.5}Mn_{0.75}Ni_{0.25}O_{2.5}$ and layered-spinel hybrids. All the cathode materials are composed of nanoparticles with dimension ranging from 50 to 200 nm. Figure 1a exhibits the octahedral-shaped particles of spinel $LiMn_{1.5}Ni_{0.5}O_4$, whereas hexagonal-shaped phase is revealed for layered structure as shown in Figure 1c. The layered-spinel material consists of the hexagonal-shaped particles and the octahedral -shaped particles (Figure 1b, d).

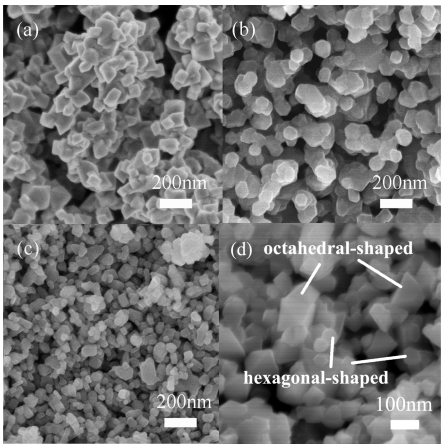


**Figure 1.** SEM images of (a) spinel $LiMn_{1.5}Ni_{0.5}O_4$, (b) layered-spinel hybrid, and (c) layered $Li_2MnO_3{-}LiMn_{0.5}Ni_{0.5}O_2$ cathode materials; (d) high-magnification image of layered-spinel hybrid, indicating the octahedral-shaped and hexagonal-shaped particles.

It is also found that the layered $Li_{1.5}Mn_{0.75}Ni_{0.25}O_{2.5}$ (Figure 1 c) has finer particles than the spinel-containing materials (Figure 1a, b). The nanostructure layered-spinel hybrid has the specific surface area of 7.4 $m^2/g$ and the average pore size is about 30 nm (see Figure S1 in the Supporting information), which is higher than 5.6 $m^2/g$ of the cathode synthesized by co-precipitation reaction,[21] thereby affording a short diffusion path for lithium ion diffusion and an increased electrode/electrolyte contact area, resulting higher specific power and better electronic/ionic conductivity.[22]

**3.2. Crystal Structure and Phase.** The crystal structure and phase of spinel, layered-spinel, and layered samples were identified with high-resolution powder XRD, as shown in Figure 2. The XRD pattern of $LiNi_{0.5}Mn_{1.5}O_4$ (Figure 2(a)) fits well to the space group of $Fd\bar{3}m$, consistent with previously reported data.[23,24] The XRD pattern of layered oxide (Figure 2(c)) fits well with $Li_{1.5}Mn_{0.75}Ni_{0.25}O_{2.5}$ structure, which has been identified as a single-phase solid solution with *C*2/*m* monoclinic symmetry and multiple planar defects by XRD and TEM.[25] Weak peaks appear in the 2$\theta$ range of 22−25° because of the ordering of the excess lithium ions in the transition metal layered of $Li_{1.5}Mn_{0.75}Ni_{0.25}O_{2.5}$.[26] The layered-spinel hybrids (Figure 2b) show reflections corresponding to layer and spinel phase. The sharp superstructure is clearly visible in the layered-spinel material, thereby reflecting the existence of $Li_2MnO_3$-based layered-spinel structure.[27,28] Raman analysis was used to examine the bonding characteristics of the layered-spinel hybrid cathode. Raman profile (see Figure S2 in the Supporting information) of the layered-spinel hybrid shows main Raman peaks at 629, 612, 583, 483, 438 $cm^{-1}$, which contain both characteristic peaks 629 $cm^{-1}$ of spinel and 612 $cm^{-1}$ of layered structure, illustrating the existence of spinel component in the hybrid. The FTIR spectra in Figure S3 (see the Supporting information) also reveals the same fact.

To explore the spinel content in the hybrid cathode, we conducted Rietveld refinements with XRD data (see Figure S4 in the Supporting Information). The details of the obtained composition of the three samples and lattice parameters of the layered phase and spinel phase are listed in Table 1. According to the refinement results the layered-spinel material has a relatively high spinel content of approximately 36 wt %, and accordingly molecular formula could be expressed as 0.64-

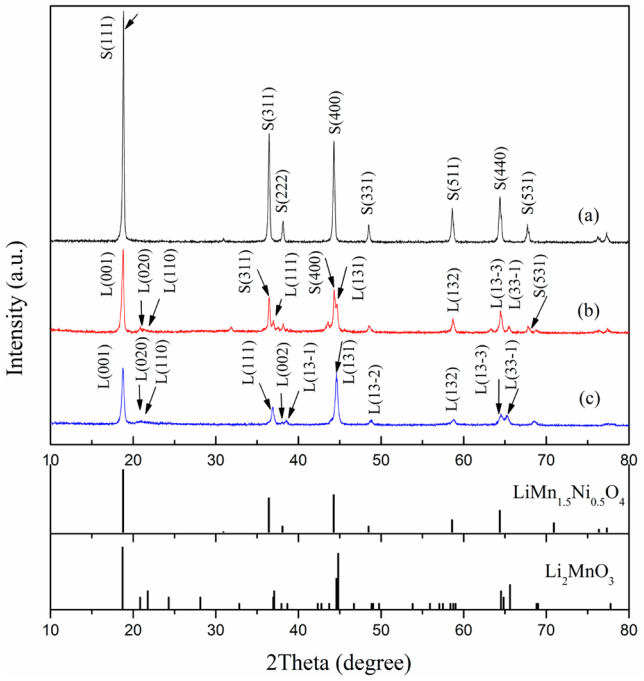


**Figure 2.** XRD patterns of cathode materials: (a) spinel $LiMn_{1.5}Ni_{0.5}O_4$, (b) layered-spinel hybrid, and (c) layered $Li_{1.5}Mn_{0.75}Ni_{0.25}O_{2.5}$ cathode materials. The standard PDF profiles of $Li_2MnO_3$ and $LiMn_{1.5}Ni_{0.5}O_4$ are shown in the figure for reference.

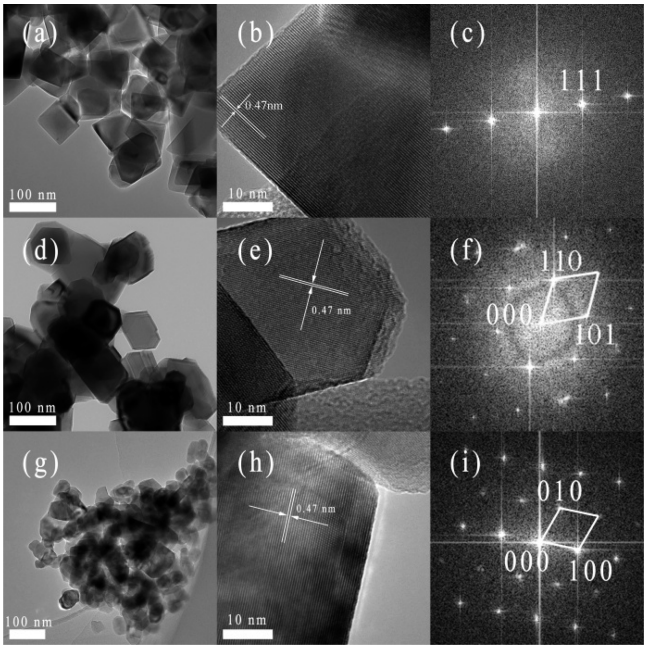


**Figure 3.** TEM images of (a, b) spinel $LiNi_{0.5}Mn_{1.5}O_4$, (d, e) layered-spinel $Li_{1.13}Mn_{0.75}Ni_{0.25}O_{2.32}$, and (g, h) layered $Li_{1.5}Mn_{0.75}Ni_{0.25}O_{2.5}$; (c, f, i) Fourier transformation (FFT) images of b, e, and h, respectively.

$[Li_{1.5}Mn_{0.75}Ni_{0.25}O_{2.5}]$-0.36 $LiNi_{0.5}Mn_{1.5}O_4$, which is corresponding to ICP result of $Li_{1.13}Mn_{0.75}Ni_{0.25}O_{2.32}$. In the spinel $LiNi_{0.5}Mn_{1.5}O_4$ sample, a very small amount (0.69 wt %) of layered phase is present due to high lithium content in the reaction.

The TEM images of spinel, layered-spinel, and layered samples are shown in Figure 3. Spinel and layered-spinel samples have more regular morphology than layered $Li_{1.5}Mn_{0.75}Ni_{0.25}O_{2.5}$. The mean size of the particles are about 100 nm, smaller than the particle size obtained by co-precipitation method, which is in favor of diffusion of lithium ion and improvement of the rate performance to some extent. Figure 3b e, and h exhibits the high-resolution images of local region in Figure 3a, d, and g. Three samples all have the same main lattice fringe distance equal to 0.47 nm, which is consistent with the characteristic plane (111) of $Fd\bar{3}m$ $LiNi_{0.5}Mn_{1.5}O_4$ or (001) plane of $C2/m$ $Li_2MnO_3$. Figure 3c, f, and i show the fast Fourier transform (FFT) patterns of Figure 3b, e, and h. It could be seen the samples are all single crystalline. The diffraction spots in image f and i in Figure 3 can be indexed to hexagonal structure for the $C2/m$ space group taken from along $[\bar{1}11]$ and [001] directions.

In addition, selected area electron diffraction (SAED) patterns and the diffraction-contrast bright-field (BF) and dark-field (DF) images were collected for the layered-spinel hybrids to clarify the two components as displayed in Figure 4.

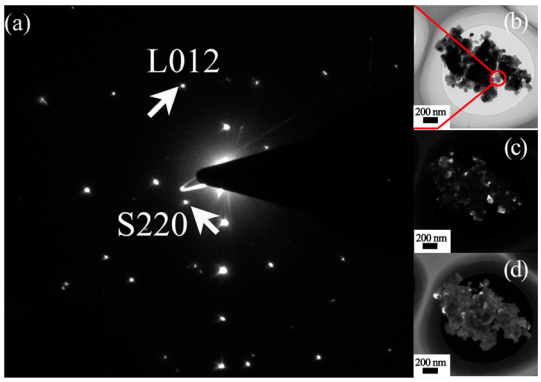


**Figure 4.** (a) Selected area electron diffraction (SAED) pattern, (b) bright-field image, (c, d) dark-field images of the layered-spinel hybrid $Li_{1.13}Mn_{0.75}Ni_{0.25}O_{2.32}$.

Figure 4a is the SAED patterns of the particles in the red circle as shown Figure 4b. The diffractions of layered plane L(012) and spinel plane S(220) are indicated by the arrows in the figure. The DF images were taken with focus on the layered nanoparticle diffraction spot L(012) and spinel diffraction spot

**Table 1. Lattice Parameters and Weight Percent of the Layered, Spinel Phase in the $xLi[Ni_{0.2}Li_{0.2}Mn_{0.6}]O_2$-$(1-x)LiMn_{1.5}Ni_{0.5}O_4$ ($x$ = 0, 0.25, 1) Cathodes**

| | wt % | | spinel ($Fd\bar{3}m$) | layered ($C2/m$) | | | |
|---|---|---|---|---|---|---|---|
| samples | spinel ($Fd\bar{3}m$) | layered | $a$ | $a$ | $b$ | $c$ | $R$ factor $R_{wp\%}$ |
| spinel ($x$ = 0) | 99.31 | 0.69 | 8.1854 | 4.9398 | 8.5029 | 5.0841 | 7.8 |
| layered-spinel ($x$ = 0.25) | 35.96 | 64.04 | 8.2429 | 4.9902 | 8.5504 | 5.0446 | 8.9 |
| layered ($x$ = 1) | 2.62 | 97.38 | 8.1679 | 4.9377 | 8.5346 | 5.0304 | 8.7 |


dx.doi.org/10.1021/am501280t | ACS Appl. Mater. Interfaces 2014, 6, 8363−8368

S(220) are shown in images c and d in Figure 4, respectively. It can be confirmed that the layered-spinel hybrid contains well dispersed $LiMn_{1.5}Ni_{0.5}O_4$ ($Fd\bar{3}m$) component. The spinel $LiM_2O_4$ (M = Mn/Li, Ni) component in the hybrid has three-dimensional space provided by $M_2O_4$ framework.[29] So the excess lithium ions can be accommodated during discharge by spinel component.[30,31]

**3.3. Electrochemical Properties.** The charge/discharge profiles at the 1st, 2nd, and 30th cycles of lithium cells containing $LiMn_{1.5}Ni_{0.5}O_4$, $Li_{1.13}Mn_{0.75}Ni_{0.25}O_{2.32}$ and $Li_{1.5}Mn_{0.75}Ni_{0.25}O_{2.5}$ electrodes recorded between 2.0 and 4.8 V at 0.1 *C* are shown in Figure 5a, c, and e, respectively. The

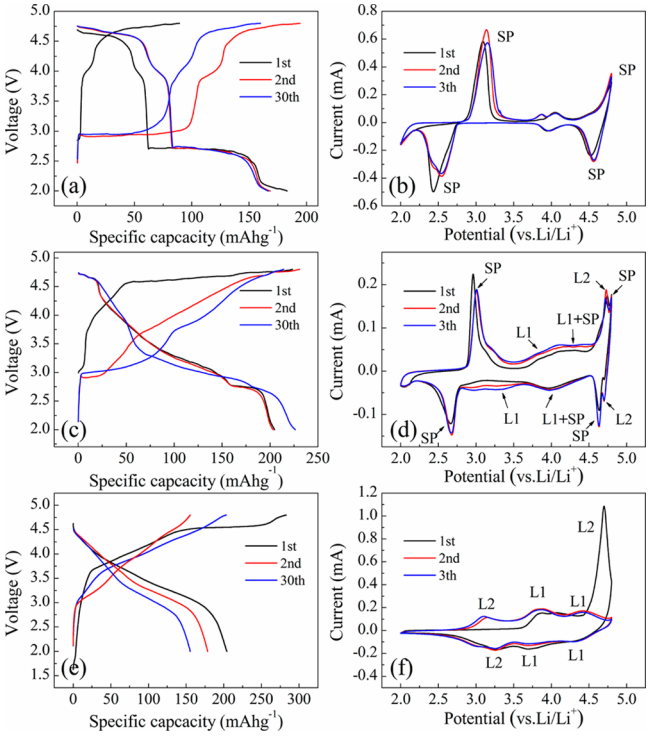


**Figure 5.** (a, c, e) Voltage profiles and (b, d, f) *C*−*V* profiles of Li cells with spinel $LiMn_{1.5}Ni_{0.5}O_4$, layered-spinel $Li_{1.13}Mn_{0.75}Ni_{0.25}O_{2.32}$, and layered $Li_{1.5}Mn_{0.75}Ni_{0.25}O_{2.5}$ electrodes.

corresponding *C*−*V* curves of the 1−3 cycles are depicted in Figure 5b, d, and f. The spinel $LiMn_{1.5}Ni_{0.5}O_4$ electrodes show four distinctive plateau regions during discharge (Figure 5(a)). The plateaus at around 4.7 and 4.0 V correspond to the extraction/insertion of lithium ion from/into 8a tetrahedral site of the cubic spinel structure. The upper plateau region at ∼4.7 V originates from the $Ni^{3+}/Ni^{4+}$ couple and the lower plateau region at ∼4.7 V corresponds to the $Ni^{2+}/Ni^{3+}$ couple.[9] The plateau region at 4.0 V originates from the $Mn^{3+}/Mn^{4+}$ couple, which is mainly due to the existence of a small amount of $Mn^{3+}$ formed during hydrothermal process.[20,32] The reaction plateaus at ∼2.8 V and ∼2.1 V are associated with the transformation of cubic to tetragonal phase during the extraction of lithium ions from empty 16c octahedral site of the cubic spinel structure.[1]

Lithium-rich layered $Li_{1.5}Mn_{0.75}Ni_{0.25}O_{2.5}$ shows distinctly different voltage curves as shown in Figure 5e. During the initial charge process, Li ion is initially extracted from the $LiMn_{0.5}Ni_{0.5}O_2$ component corresponding to the oxidation of the transition metal $Ni^{2+}$ to $Ni^{4+}$ at about 4.0 V.[31] Thereafter between 4.5 and 4.8 V, lithium and oxygen are removed irreversibly from $Li_2MnO_3$ with a net loss of $Li_2O$, resulting in a layered structure $MnO_2$.[32] During the subsequent discharge, there are three reduction peaks at ∼4.3, ∼3.7, and ∼3.3 V (Figure 5f). Lithium ion first inserts into $Mn_{0.5}Ni_{0.5}O_2$ at approximately 4.3 to 3.7 V ($Ni^{4+}$ to $Ni^{2+}$), and then into the $MnO_2$ derived from $Li_2MnO_3$ at 3.3 V ($Mn^{4+}$ to $Mn^{3+}$).[14] In the second cycle, the *C*−*V* profile is different from those observed in the first cycle. The strong peak at 4.7 V disappears and a weak new peak turns up at 4.4 V, indicating the oxidation peak above 4.5 V is irreversible. The reversible redox of the Mn ions blow 3.5 V can be still observed in the second cycle.

Layered-spinel $Li_{1.13}Mn_{0.75}Ni_{0.25}O_{2.32}$ profiles exhibit both spinel and layered characteristics as shown in Figure 5(c). The voltage plateaus between 3.7 and 4.5 V in Figure 5d are attributed to the extraction of lithium ion from layered $LiMn_{0.5}Ni_{0.5}O_2$.[5] When charging to 4.6 V, the removal of $Li_2O$ from the electrode structure occurs. The reaction plateau at ∼2.8 V is obviously associated with the reduction of $Mn^{4+}$ to $Mn^{3+}$ in the spinel $LiMn_{1.5}Ni_{0.5}O_4$ component.[12] But the plateau at 2.1 V becomes less evident due to small amount of spinel content compare to layered phase. The result corresponding to the *C*−*V* curves in Figure 5d highlights the complexity of the electrochemical processes occurred in layered-spinel composite structure, in which the layered component concluding $LiMn_{0.5}Ni_{0.5}O_2$ (L1) and $Li_2MnO_3$ (L2) and spinel $LiMn_{1.5}Ni_{0.5}O_4$ (SP) component can be identified.

The cyclability in terms of discharge capacity of spinel $LiMn_{1.5}Ni_{0.5}O_4$, layered-spinel hybrids and layered $Li_2MnO_3$−$LiMn_{0.5}Ni_{0.5}O_2$ between 2 and 4.8 V at 0.1 *C* is shown in Figure 6a. The spinel electrode delivers 181 mAh $g^{-1}$ for the first cycle and keeps increasing gradually under the following cycles. The layered electrode shows 201 mAh $g^{-1}$ for the initial cycle but decreases regularly in the following cycles. Layered-spinel hybrid cathode shows the first discharge capacity of 218 mAh $g^{-1}$. However, the capacity of layered-spinel hybrids increases steadily on the cycling and attains a stable reversible capacity of about 240 mAh $g^{-1}$ after the third cycle. The continuously increasing capacity is attributed to the 3 V spinel-like phase from the lithium-rich layered phase.[9]

Figure 6b provides a comparison of the rate performance of spinel, layered-spinel, and layered electrodes. The cell was initially cycled 3 times under a *C*/10 rate to activate the electrode material and then cycled under a charge rate of *C*/10 and discharge rates of *C*/10, *C*/2, 1 *C*, 2 *C*, and 5 *C* in sequence for 5 cycles each. The data indicate that the performance of layered-spinel electrode is much better than the other electrodes. At 1 *C*, layered-spinel electrode delivers about 140 mAh $g^{-1}$, whereas layered and spinel deliver 108 and 92 mAh $g^{-1}$ at the same rate, respectively. When the current rate returns to 0.1 *C* from 5 *C*, the capacity of layered-spinel sample remains almost the same value of the initial discharge capacity at 0.1 *C*, which indicates the sample has good rate performance. Under our experiment conditions the rate performance of layered-spinel electrode is greatly improved compared with layered electrode. The improved rate performance is attributed to the nanosized particles and three-dimensional spinel phase. It is worth noting that the discharge capacities of all the samples tend toward a same level while the discharge rate increases from 0.1 to 5 *C*, indicating the diffusion of lithium-ion in the layered and the spinel structure may become the same at higher discharge rates.


dx.doi.org/10.1021/am501280t | ACS Appl. Mater. Interfaces 2014, 6, 8363−8368

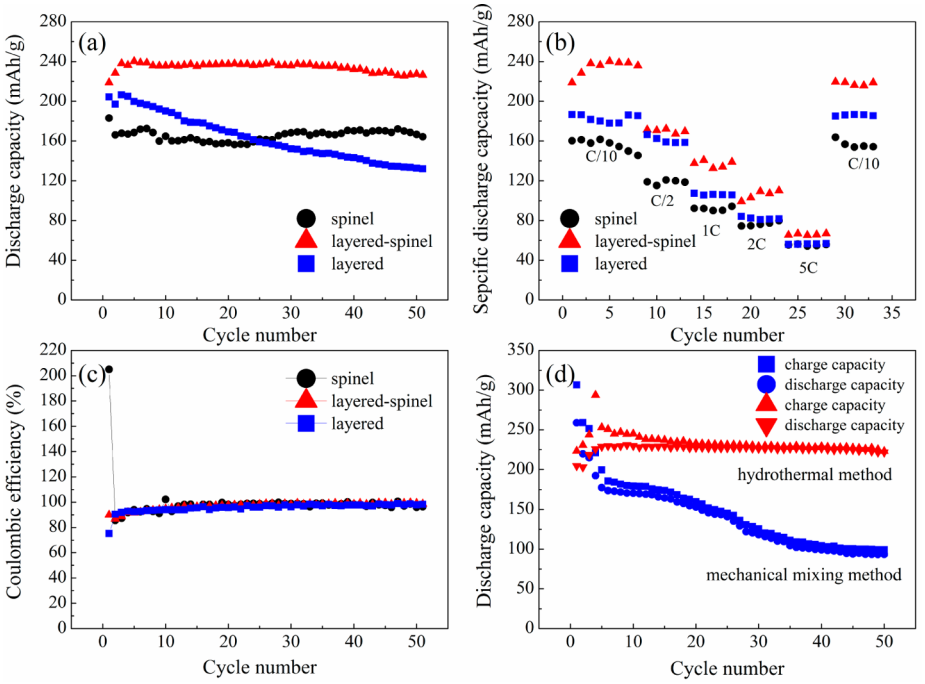


**Figure 6.** Electrochemical performance of the spinel electrode, layered-spinel and layered electrode (a) cycle performance under charge rate of *C*/10 and discharge rate of *C*/10; (b) rate performance under charge rate *C*/10 and discharge *C*/10, *C*/2, 1*C*, 2*C*, 5*C*; (c) coulombic efficiencies during 50 cycles when cycled under *C*/10; (d) layered-spinel electrode prepared by different methods.

The coulombic efficiencies of spinel, layered-spinel and layered samples during 50 cycles between 2 and 4.8 V at 0.1C are shown in Figure 6c. The spinel electrode gets the highest first coulombic efficiency of 205% (>100%) because of the insertion of additional lithium ions into the empty 16c octahedral site of the spinel phase. On the other hand, the layered cathode shows the lowest coulombic efficiency of 75% due to the net loss of $Li_2O$ and the inability to insert all the lithium back into the layered lattice.[25] The layered-spinel hybrids show improved coulombic efficiency of 90%, and this is mainly attributed to the spinel component in the cathode, which can accommodate the oversupply of lithium from the $Li_2MnO_3$ component on the initial charge, the spinel component can stable the layered phase by improving first-cycle efficiency.[8] The spinel content in hybrids is expected to be controlled by adjusting hydrothermal parameter, which is still in progress in our laboratory.

Comparison of the cycling stability in terms of discharge capacity of the layered-spinel cathodes synthesized by hydrothermal method discussed previously and by mechanical mixing method is shown in Figure 6d. It could be clearly seen that the electrode prepared by hydrothermal method has superior cyclability than the mechanical mixed hybrid cathode. The mechanical mixing electrode shows relatively high discharge capacity during the first two cycles, whereas it decays seriously in the following cycles. The reason is attributed to the spinel component well-dispersed in the composite and the good combination between layered and spinel component during hydrothermal processing.

## 4. CONCLUSIONS

Nanosized layered-spinel composite cathode $Li_{1.13}Mn_{0.75}Ni_{0.25}O_{2.32}$ was synthesized by a hydrothermal approach followed by calcination. The samples are proven to have uniformly distributed nanoparticles of 50−200 nm by SEM and TEM, which may be in favor of diffusion of lithium ion and improvement of the rate performance. To be used as a cathode for lithium ion battery, the hybrid exhibits an excellent cycle performance: the first-cycle efficiency of the layered-spinel composite cathode is improved from 71 to 90% by integrating spinel component and it maintained quite good cycling stability at 0.1 *C* with the capacity retention of 94.6% after 100 cycles, which made this hybrid cathode a very promising candidate for the application of rechargeable Li-ion batteries in HEVs.

## ■ ASSOCIATED CONTENT

### Ⓢ Supporting Information

Pore size distribution of the layered-spinel hybrid and Raman spectra, FTIR spectra, and Rietveld refinement results of layered $Li_{1.5}Mn_{0.75}Ni_{0.25}O_{2.5}$, layered-spinel $Li_{1.13}Mn_{0.75}Ni_{0.25}O_{2.32}$ and spinel $LiMn_{1.5}Ni_{0.5}O_4$. This material is available free of charge via the Internet at http://pubs.acs.org.

## ■ AUTHOR INFORMATION

### Corresponding Author

*E-mail: csshi@tju.edu.cn.

### Notes

The authors declare no competing financial interest.

## ■ ACKNOWLEDGMENTS

The authors acknowledge the financial supports by China-EU Science and Technology Cooperation Project (1206), and the Key Technologies R & D Program of Tianjin (12ZCZDGX00800).

## ■ REFERENCES

(1) Park, S.; Kang, S.; Johnson, C.; Amine, K.; Thackeray, M. Lithium−Manganese−Nickel-Oxide Electrodes with Integrated Layered−Spinel Structures for Lithium Batteries. *Electrochem. Commun.* **2007**, *9*, 262−268.

(2) Ji, G.; Ma, Y.; Lee, J. Y. Mitigating the Initial Capacity Loss (ICL) Problem in High-Capacity Lithium Ion Battery Anode Materials. *J. Mater. Chem.* **2011**, *21*, 9819−9824.
(3) Lu, Z. H.; MacNeil, D. D.; Dahn, J. R. Layered Li-$[Ni_xCo_{1-2x}Mn_x]O_2$ Cathode Materials for Lithium-Ion Batteries. *Electrochem. Solid-State Lett.* **2001**, *4*, A200−A203.
(4) Lu, Z. H.; MacNeil, D. D.; Dahn, J. R. Layered Li-$[Ni_xLi_{(1/3-2x/3)}Mn_{(2/3-x/3)}]O_2$ Cathode Materials for Lithium-Ion Batteries. *Electrochem. Solid-State Lett.* **2001**, *4*, A191−A194.
(5) Shin, S. S.; Sun, Y. K.; Amine, K. Synthesis and Electrochemical Properties of $Li[Li_{(1-2x)/3}Ni_xMn_{(2-x)/3}]O_2$ as Cathode Materials for Lithium Secondary Batteries. *J. Power Sources* **2002**, *112*, 634−638.
(6) Kang, S. H.; Sun, Y. K.; Amine, K. Electrochemical and *ex Situ* X-Ray Study of $Li(Li_{0.2}Ni_{0.2}Mn_{0.6})O_2$ Cathode Material for Li Secondary Batteries. *Electrochem. Solid-State Lett.* **2003**, *6*, A183−A186.
(7) Yabuuchi, N.; Yoshii, K.; Myung, S. T.; Nakai, I.; Komaba, S. Detailed Studies of a High-Capacity Electrode Material for Rechargeable Batteries, $Li_2MnO_3$−$LiCo_{1/3}Ni_{1/3}Mn_{1/3}O_2$. *J. Am. Chem. Soc.* **2011**, *133*, 4404−4419.
(8) Kim, D.; Sandi, G.; Croy, J. R.; Gallagher, K. G.; Kang, S. H.; Lee, E.; Slater, M. D.; Johnson, C. S.; Thackeray, M. M. Composite 'Layered-Layered-Spinel' Cathode Structures for Lithium-Ion Batteries. *J. Electrochem. Soc.* **2013**, *160*, A3−A38.
(9) Lee, E. S.; Huq, A.; Chang, H. Y.; Manthiram, A. High-Voltage, High-Energy Layered-Spinel Composite Cathodes with Superior Cycle Life for Lithium-Ion Batteries. *Chem. Mater.* **2012**, *24*, 600−612.
(10) Cabana, J.; Kang, S. H.; Johnson, C. S.; Thackeray, M. M.; Grey, C. P. Structural and Electrochemical Characterization of Composite Layered-Spinel Electrodes Containing Ni and Mn for Li-Ion Batteries. *J. Electrochem. Soc.* **2009**, *156*, A730−A736.
(11) Kim, M. G.; Jo, M.; Hong, Y. S.; Cho, J. Template-Free Synthesis of $Li[Ni_{0.25}Li_{0.15}Mn_{0.6}]O_2$ Nanowires for High Performance Lithium Battery Cathode. *Chem. Commun.* **2009**, 218−220.
(12) Deng, H.; Belharouak, I.; Cook, R. E.; Wu, H.; Sun, Y. K.; Amine, K. Nanostructured Lithium Nickel Manganese Oxides for Lithium-Ion Batteries. *J. Electrochem. Soc.* **2010**, *157*, A447−A452.
(13) Wei, G. Z.; Lu, X.; Ke, F. S.; Huang, L.; Li, J. T.; Wang, Z. X.; Zhou, Z. Y.; Sun, S. G. Crystal Habit-Tuned Nanoplate Material of $Li[Li_{1/3-2x/3}\ Ni_xMn_{2/3-x/3}]O_2$ for High-Rate Performance Lithium-Ion Batteries. *Adv. Mater.* **2010**, *22*, 4364−4367.
(14) Kim, J. S.; Johnson, C. S.; Vaughey, J. T.; Thackeray, M. M. Electrochemical and Structural Properties of $xLi_2M'O_3\cdot(1-x)$-$LiMn_{0.5}Ni_{0.5}O_2$ Electrodes for Lithium Batteries (M′ = Ti, Mn, Zr; $0 \le x \le 0.3$). *Chem. Mater.* **2004**, *16*, 1996−2006.
(15) Johnson, C. S.; Li, N.; Vaughey, J. T.; Hackney, S. A.; Thackeray, M. M. Lithium−Manganese Oxide Electrodes with Layered−Spinel Composite Structures $xLi_2MnO_3\cdot(1-x)Li_{1+y}Mn_{2-y}O_4$ ($0 < x < 1$, $0 \le y \le 0.33$) for Lithium. Batteries. *Electrochem. Commun.* **2005**, *7*, 528−536.
(16) Kim, D.; Kang, S. H.; Balasubramanian, M.; Johnson, C. S. High-Energy and High-Power Li-Rich Nickel Manganese Oxide Electrode Materials. *Electrochem. Commun.* **2010**, *12*, 1618−1621.
(17) Croy, J. R.; Kang, S. H.; Balasubramanian, M.; Thackeray, M. M. $Li_2MnO_3$-Based Composite Cathodes for Lithium Batteries: A Novel Synthesis Approach and New Structures. *Electrochem. Commun.* **2011**, *13*, 1063−1066.
(18) Sim, C. M.; Kim, J. H.; Hong, Y. J.; Lee, J. K.; Kang, Y. C. Electrochemical Characteristics of Layered-Spinel $0.7Li_2MnO_30.3Li_4Mn_5O_{12}$ Composite Powders with Spherical Shape and Porous Nanostructure. *Int. J. Electrochem. Sci.* **2013**, *8*, 4850−4863.
(19) Zhang, X. F.; Lengyel, M.; Axelbaum, R. L. Nanostructured High-Energy $xLi_2MnO_3\cdot1$-$xLiNi_{0.5}Mn_{0.5}O_2(0.3\le x\le0.6)$ Cathode Materials. *AIChE J.* **2014**, *60*, 443−450.
(20) Huang, X.; Zhang, Q.; Chang, H.; Gan, J.; Yue, H.; Yang, Y. J. Hydrothermal Synthesis of Nanosized $LiMnO_2$-$Li_2MnO_3$ Compounds and Their Electrochemical Performance. *Electrochem. Soc.* **2009**, *156*, A162−A168.
(21) Wang, D.; Belharouak, I.; Zhou, G.; Amine, K. Nanoarchitecture Multi-Structual Cathode Materials for High Capacity Lithium Batteries. *Adv. Funct. Mater.* **2013**, *23*, 1070−1075.
(22) Zheng, J. M.; Wu, X. B.; Yang, Y. A. Comparison of Preparation Method on The Electrochemical Performance of Cathode Material $Li[Li_{0.2}Mn_{0.54}Ni_{0.13}Co_{0.13}]O_2$ for Lithium Ion Battery. *Electrochim. Acta* **2011**, *56*, 3071−3078.
(23) Kunduraci, M.; Amatucci, G. G. Synthesis and Characterization of Nanostructured 4.7 V $LixMn_{1.5}Ni_{0.5}O_4$ Spinels for High-Power Lithium-Ion Batteries. *J. Electrochem. Soc.* **2006**, *153*, A1345.
(24) Talyosef, Y.; Markovsky, B.; Lavi, R.; Salitra, G.; Aurbach, D.; Kovacheva, D.; Gorova, M.; Zhecheva, E.; Stoyanova, R. Comparing the Behavior of Nano- and Microsized Particles of $LiMn_{1.5}Ni_{0.5}O_4$ Spinel as Cathode Materials for Li-Ion Batteries. *J. Electrochem. Soc.* **2007**, *154*, A682−691.
(25) Jarvis, K. A.; Deng, Z.; Allard, L. F.; Manthiram, A.; Ferreira, P. Atomic Structure of a Lithium-Rich Layered Oxide Material for Lithium-Ion Batteries: Evidence of a Solid Solution. *J. Chem. Mater.* **2011**, *23*, 3614−3621.
(26) Bréger, J.; Jiang, M.; Dupré, N.; Meng, Y. S.; Shao-Horn, Y.; Ceder, G.; Grey, C. P. High-Resolution X-ray Diffraction, DIFFaX, NMR and First Principles Study of Disorder in the $Li_2MnO_3$-$Li[Ni_{1/2}Mn_{1/2}]O_2$ Solid Solution. *J. Solid State Chem.* **2005**, *178*, 2575−2585.
(27) Meng, Y. S.; Ceder, G.; Grey, C. P.; Yoon, W. S.; Jiang, M.; Bréger, J.; Shao-Horn, Y. Cation Ordering in Layered O3 Li-$[Ni_xLi_{1/3-2x/3}Mn_{2/3-x/3}]O_2$ ($0 \le x \le 1/2$) Compounds. *Chem. Mater.* **2005**, *17*, 2386−2394.
(28) Huang, X.; Zhang, Q.; Gan, J.; Chang, H.; Yang, Y. Hydrothermal Synthesis of a Nanosized $LiNi_{0.5}Mn_{1.5}O_4$ Cathode Material for High Power Lithium-Ion Batteries. *J. Electrochem. Soc.* **2011**, *158*, A139−A145.
(29) Amine, K.; Liu, J.; Belharouak, I.; Kang, S. H.; Bloom, I.; Vissers, D.; Henriksen, G. Advanced Cathode Materials for High-Power Applications. *J. Power Sources* **2005**, *146*, 111−115.
(30) Wu, Y.; Manthiram, A. Effect of Surface Modifications on the Layered Solid Solution Cathodes $(1-z)Li[Li_{1/3}Mn_{2/3}]$-$(z)Li[Mn_{0.5-y}Ni_{0.5-y}Co_{2y}]O_2$. *Solid State Ionics* **2009**, *180*, 50−56.
(31) Armstrong, A. R.; Holzapfel, M.; Novák, P.; Johnson, C. S.; Kang, S. H.; Thackeray, M. M.; Bruce, P. G. Demonstrating Oxygen Loss and Associated Structural Reorganization in the Lithium Battery Cathode $Li[Ni_{0.2}Li_{0.2}Mn_{0.6}]O_2$. *J. Am. Chem. Soc.* **2006**, *128*, 8694−8698.
(32) Amine, K.; Tukamoto, H.; Yasuda, H.; Fujita, Y. A New Three-Volt Spinel $Li_{1+x}Mn_{1.5}Ni_{0.5}O_4$ for Secondary Lithium Batteries. *J. Electrochem. Soc.* **1996**, *143*, 1607−1613.